ACCSCIENCE PUBLISHING

International Journal of Bioprinting

RESEARCH ARTICLE

3D-printed biodegradable hydrogel microrobots for controlled therapeutic delivery

Pan Liao[1,2,3]*, Junyang Li[2], Shuxun Chen[2], Yi Hou[4]*, Guangda Zhu[3]*, and Dong Sun[2]

[1] Laoshan Laboratory, Qingdao, Shandong, China

[2] Department of Biomedical Engineering, City University of Hong Kong, Hong Kong, China

[3] Research Center for Materials, Architectures, and Integration of Nanomembranes, TU Chemnitz, Chemnitz, Germany

[4] Centre for Translational Bone, Joint and Soft Tissue Research, TU Dresden, Dresden, Germany

Abstract

Precise delivery of therapeutic agents to targeted sites within the body is a significant challenge, especially in complex and confined physiological environments. Magnetically actuated microrobots offer a promising solution by enabling remote, controllable, and minimally invasive navigation; however, most existing microrobotic systems are fabricated from nondegradable materials and lack controlled drug release capability, which significantly limits their clinical translation. Here, we report 3D-printed biodegradable magnetic microrobots based on gelatin methacryloyl (GelMA) hydrogel capable of controlled therapeutic delivery. Using high-resolution direct laser writing, dual-layer GelMA microrobots with distinct crosslinking degrees were fabricated, enabling tunable degradation and controlled release of encapsulated drugs. The low-crosslinked outer shell functions as a protective barrier that prevents premature drug diffusion, while the highly crosslinked inner core enables sustained drug release during enzymatic degradation. The microrobots demonstrate excellent biocompatibility and controllable degradation in cellular environments. In addition, the integration of a biocompatible magnetic skeleton within the GelMA body enhances mechanical stability and enables precise magnetic actuation. This study presents a versatile strategy for developing biodegradable, magnetically actuated microrobots with controlled therapeutic release, offering strong potential for targeted drug delivery, tissue regeneration, and minimally invasive biomedical applications.

Keywords: Biodegradable microrobots; Controlled drug release; Direct laser writing; Magnetic actuation; Targeted therapy

***Corresponding authors:**
Pan Liao (pliao@lsnl.cn)

Yi Hou (houyicool@iccas.ac.cn)

Guangda Zhu (zhuguangda@iccas.ac.cn)

Citation: Liao P, Li J, Chen S, Hou Y, Zhu G, Sun D. 3D-printed biodegradable hydrogel microrobots for controlled therapeutic delivery. *Int J Bioprint*. 2026;12(1):385-397. doi: 10.36922/IJB025460475

Received: November 14, 2025
Revised: November 30, 2025
Accepted: December 2, 2025
Published online: December 2, 2025

1. Introduction

The active transport and precise delivery of drugs, genes, and vaccines to specific sites within the body hold great potential for a wide range of biomedical applications, including targeted therapy, tissue repair and regeneration, and effective vaccination.[1-5] However, achieving accurate delivery of these therapeutics to diseased sites, particularly

within complex and confined regions of the body such as the gastrointestinal tract, brain, and spinal cord, remains a major challenge.[6–8] Microrobots, with characteristic sizes ranging from several to hundreds of micrometers, offer a promising solution by enabling active navigation and targeted transport of therapeutic agents into these inaccessible regions of the human body.[9–15] In particular, magnetically actuated microrobots have attracted increasing attention in the biomedical field due to their wireless controllability, high positioning precision, and noninvasive therapeutic potential,[16–21] with significant progress demonstrated in applications such as thrombus ablation and biofilm removal from tympanostomy tubes and biliary stents.[22–27]

Targeted therapeutic agents are typically incorporated into biocompatible magnetic microrobots through either surface functionalization or encapsulation within the microrobot body.[28–33] Surface-functionalized microrobots loaded with various drugs can achieve stimulus-responsive release[33–37]; however, most of these systems are fabricated from nonbiodegradable materials, which may induce inflammatory responses or other adverse biological effects. In contrast, biocompatible and biodegradable microrobots allow therapeutic payloads to be directly encapsulated within their structural matrix, thereby enhancing loading efficiency and enabling controlled, sustained release through gradual degradation under physiological conditions.[38–41] Among biodegradable materials, gelatin methacryloyl (GelMA) stands out as a particularly promising candidate due to its excellent cytocompatibility, intrinsic bioactivity, and enzymatic degradability.[42–44] GelMA-based magnetic microrobots, including enzymatically degradable microswimmers, have demonstrated remarkable potential for targeted drug or cell transport and localized therapy.[38,45–47] Recent advances in gelatin-based magnetic microrobots have enabled the integration of electromagnetic navigation, release catheters, and dissolvable drug-loaded capsules, demonstrating effective navigation in human vasculature models and successful tracking in large-animal studies.[48] Moreover, the therapeutic efficacy depends on both delivery precision and release kinetics.[1,49–52] Premature or uncontrolled release of encapsulated agents caused by early degradation of the microrobots before reaching the target site can severely compromise therapeutic performance. Therefore, achieving spatiotemporally controlled drug release is essential to ensure on-demand therapeutic action while minimizing premature drug leakage during navigation. However, the development of magnetic microrobots that combine precise actuation, tunable biodegradation, and controlled drug release remains a challenge.

Herein, we present 3D-printed biocompatible and biodegradable GelMA-based magnetic microrobots with controllable delivery capability. The microrobots are fabricated using high-resolution direct laser writing (DLW) based on two-photon polymerization and feature a dual-layer architecture with distinct crosslinking degrees (Figure 1A), enabling tunable degradation behavior for controlled drug release. The low-crosslinked outer GelMA shell serves as a protective barrier that prevents premature drug loss, while the highly crosslinked GelMA inner core allows sustained, on-demand release of therapeutic agents, thereby improving overall delivery efficiency. The microrobots exhibit excellent biocompatibility, undergoing gradual degradation during co-culture with MC3T3 cells and complete degradation in a trypsin–EDTA enzymatic medium. Furthermore, a biocompatible magnetic skeleton is embedded within the GelMA body to enable magnetic actuation (Figure 1B). The incorporation of this magnetic skeleton enhances mechanical integrity and provides precise, responsive magnetic control, allowing reliable detachment of printed microrobots from the printing substrate and stable operation under an external magnetic field. Overall, this design strategy establishes a versatile platform for developing next-generation biodegradable microrobots that integrate magnetic navigation, tunable biodegradation, and controlled therapeutic release, offering new opportunities for targeted drug delivery, tissue regeneration, and precision medicine.

2. Materials and methods

2.1. Preparation of biodegradable hydrogel precursor

The biodegradable hydrogel precursor was prepared by dissolving 100 mg of gelatin methacryloyl (GelMA), 25 mg of lithium phenyl-2,4,6-trimethylbenzoylphosphinate (LAP), and 50 mg of polyethylene glycol (PEG, 50% in H_2O, M_W = 4000) in 950 μL of phosphate-buffered saline (PBS). The resulting solution was stored at 4°C prior to use. For fluorescence imaging, 1 mg of Rhodamine B-PEG-Thiol (RB-PEG-SH) was added when required.

2.2. Preparation of magnetic precursor

The magnetic precursor used for fabricating the magnetic skeleton was prepared by dissolving 50 mg of photoinitiator Easepi EDB, 10 mg of photosensitizer 2-isopropyl-9H-thioxanthen-9-one (Easepi ITX), and 20 μL of Fe_3O_4 magnetic nanoparticles (MNPs; 100 nm, 260 mg/mL in γ-butyrolactone) in a mixture of 0.5 mL poly(ethylene glycol) diacrylate (PEGDA, M_n = 575) and 0.5 mL pentaerythritol tetraacrylate (PETA). The mixture was vortexed and shaken at 300 rpm for at least 30 min until a uniform dispersion was obtained.

2.3. 3D printing of dual-layer GelMA microstructures and magnetic microrobots

Before printing, the GelMA precursor was liquefied by incubation in a 37°C deionized water bath for 10 min and then deposited onto a glass substrate for DLW. The GelMA microstructures were fabricated using a commercial DLW system (Photonic Professional GT, Nanoscribe GmbH) equipped with a 63× oil-immersion objective (NA = 1.4) and a 780 nm femtosecond laser. After printing, the samples were developed in deionized water at 40°C for 10 min to remove unpolymerized precursor. Dual-layer GelMA microstructures were fabricated by repeating the GelMA printing process. The alignment of different layers was achieved using the built-in interface finder along the Z-axis and marker-based positioning along the XY-axis. The magnetic microrobots, consisting of a magnetic skeleton (see Figure S1) and a GelMA body, were produced following the same procedure. After fabrication, all microrobots were stored in PBS at 4°C until further use. For the dual-layer GelMA microstructures, we trimmed a small portion from the bottom of each sphere to create a flat contact area to enhance adhesion between the spherical microrobots and the substrate during fabrication (see Figure S2). For the magnetic microrobots with a magnetic skeleton, the printed skeleton already adheres well to the substrate, and thus no additional design modifications are required.

2.4. Cell culture and cytocompatibility evaluation

In this experiment, MC3T3-E1 cells (ATCC CRL-2594) obtained from American Type Culture Collection (ATCC) were used. The cells were cultured in Dulbecco's Modified Eagle Medium (DMEM) supplemented with 10% fetal bovine serum (FBS) and 1% penicillin–streptomycin, and maintained at 37°C in a humidified 5% CO_2 incubator. For cytocompatibility evaluation, GelMA microstructures were co-cultured with MC3T3-E1 cells in standard growth medium, and the morphology of both cells and microstructures was monitored at predetermined time points using phase-contrast microscopy. Upon reaching confluency, cells were treated with 125 μg/mL trypsin–EDTA to induce GelMA degradation and promote cargo release. All images were acquired using an inverted fluorescence microscope (Ts2R-FL, Nikon).

2.5. Drug loading

GelMA microstructures were lyophilized overnight using a freeze dryer (FD-10-ME, Labfreez). DNA plasmid (2 μg) was mixed with 10 μL of transfection reagent (Lipofectamine™ 2000) and diluted in 100 μL PBS. The resulting DNA–lipoplex solution was added to the dried microstructures and incubated overnight. After incubation, the microstructures were washed three times with PBS and subsequently co-cultured with MC3T3-E1 cells for gene transfection and protein expression. Fluorescence images were obtained using an inverted fluorescence microscope (Ts2R-FL, Nikon).

2.6. Enzymatic degradation

Dual-layer GelMA microstructures with different crosslinking degrees were fabricated to investigate their enzymatic degradation behavior. The samples were incubated in PBS containing 12.5 mg/mL trypsin–EDTA, and the degradation process was monitored using a confocal laser scanning microscope (TCS SP8, Leica Microsystems). Fluorescent images were captured at defined time intervals and analyzed using Fiji–ImageJ software (National Institutes of Health, USA).

2.7. Magnetic actuation of microrobots

The magnetic microrobots were actuated using a permanent magnet. A cubic neodymium iron boron (NdFeB) magnet with dimensions of 50 mm × 30 mm × 5 mm and a field strength of approximately 70 mT was used, and the working distance was kept below 50 mm. The locomotion behavior under magnetic stimulation was observed and recorded using an optical microscope.

2.8. Statistical analysis

All experiments were performed in triplicate. Statistical and graphical analyses were conducted in Excel using data, including fluorescence intensity measurements, exported from the Fiji–ImageJ software (National Institutes of Health, USA). All data are presented as mean ± standard deviation.

3. Results and discussion

3.1. Design of biodegradable hydrogel microrobots

To achieve controlled therapeutic delivery, we designed biodegradable dual-layer GelMA microstructures and magnetically actuated microrobots with precise structural and functional tunability (Figure 1A and 1B). The microrobots were constructed with a spherical geometry to ensure isotropic homogeneity during fabrication and operation. For the dual-layer GelMA microstructures, the diameters of each layer can be precisely tuned to achieve different drug release profiles. In this study, the diameters of the inner core and the outer shell were set to 30 μm and 50 μm, respectively (Figure 1A). The dual-layer GelMA microstructures were fabricated using DLW based on two-photon polymerization, a high-resolution 3D printing technique that provides submicron precision and accurate spatial control of polymerization, allowing multi-material integration through sequential printing.[53–57] Using this approach, dual-layer GelMA microstructures with distinct crosslinking degrees and magnetic microrobots

composed of different materials were fabricated. GelMA hydrogel precursors (Figure 1C) were employed as the printing material for the microrobot body because of their excellent biocompatibility, intrinsic bioactivity, and enzymatic degradability.[42–44] As a proteolytically degradable biomaterial, GelMA has been widely used for controlled drug delivery, cell encapsulation, and tissue engineering applications, serving as a versatile scaffold for supporting cell proliferation and differentiation.[58–60] In parallel, the magnetic skeleton (Figure 1B) was fabricated from a magnetic precursor containing poly(ethylene glycol) diacrylate (PEGDA), pentaerythritol tetraacrylate (PETA), and Fe_3O_4 MNPs (Figure 1C), consistent with our previous work.[5,24] The PEGDA–PETA matrix provides both mechanical robustness and degradability, while the incorporation of Fe_3O_4 MNPs imparts magnetic responsiveness, enabling remote and precise actuation of the microrobots.

Figure 1D schematically illustrates the sequential fabrication process of the dual-layer GelMA microstructures using direct laser writing (DLW). The GelMA core with a high crosslinking degree was first printed within a droplet of hydrogel precursor solution at a high laser power (Figure 1D (i)) and then developed in a 37°C deionized water bath for 5 minutes to remove unpolymerized residues. The cleaned and dried microstructures were then coated with a second droplet of hydrogel precursor and realigned with the original coordinates for the subsequent printing step (Figure 1D (ii)). The outer shell was printed at a lower laser power to achieve a lower crosslinking density, forming a degradable layer that serves as a protective barrier to prevent premature drug loss. This sequential process allows the precise fabrication of dual-layer GelMA microstructures with well-defined interfaces and accurately controlled structural dimensions, as illustrated in Figure 1D (iii). Figure 1E schematically presents the fabrication workflow of the magnetically actuated microrobots composed of a magnetic skeleton (see Figure S1 for detailed structural parameters) and a GelMA body. The magnetic skeleton, composed of PEGDA, PETA, and Fe_3O_4 MNPs, was first printed, followed by printing the GelMA body using the same sequential fabrication approach as for printing the dual-layer GelMA microstructures. This dual-material 3D printing strategy provides a flexible and efficient route to integrate biodegradability, biocompatibility, and magnetic actuation within a single microrobotic platform. The resulting fabrication methodology establishes a robust foundation for creating functional microrobots with tunable degradation, controlled drug release, and precise magnetic responsiveness, offering significant potential for targeted therapeutic delivery and minimally invasive biomedical applications.

3.2. Fabrication and tunable degradability of dual-layer GelMA microstructures

First, the controlled degradability of the 3D-printed dual-layer GelMA structures with varying crosslinking degrees was investigated. Figure 2A schematically illustrates the designed structure of the dual-layer GelMA microstructures, accompanied by bright-field and fluorescence microscopy images confirming successful fabrication. The inner core and outer shell have diameters of 30 μm and 50 μm, respectively. The core, containing rhodamine B, exhibits red fluorescence, whereas the outer shell, containing FITC, emits green fluorescence (Figure 2A). To achieve sustained and programmable release, GelMA microstructures were designed with two layers exhibiting distinct crosslinking degrees (Figure 2B). Such structures can be fabricated by tuning the DLW parameters, particularly the laser power, which determines the crosslinking density and thereby controls the degradation kinetics and release behavior of the encapsulated cargo. Highly crosslinked GelMA networks contain fewer water molecules and exhibit lower permeability to surrounding aqueous media, effectively minimizing premature drug diffusion. As enzymatic degradation proceeds, the polymer network gradually loosens, leading to an increase in mesh size that facilitates drug diffusion and release. In contrast, low-crosslinked GelMA hydrogels possess larger initial mesh sizes, resulting in faster degradation and more rapid cargo release. Therefore, constructing microrobots with layers of varying crosslinking degrees enables stepwise degradation and controlled, sustained drug release. We selected laser powers of 30, 45, and 60 mW because these values produced GelMA microstructures with good mechanical stability while offering distinct crosslinking levels. At lower laser powers, insufficiently crosslinked structures were too soft to maintain their spherical geometry in air. Conversely, excessively high laser powers easily induced cavitation bubbles during scanning, leading to deformation of the printed GelMA microstructures. The combination of 30, 45, and 60 mW laser powers with a scanning speed of 5 mm/s was therefore optimal for fabricating stable GelMA microstructures with controlled crosslinking gradients. Figure 2C and 2D show the degradation and release behavior of the printed dual-layer GelMA microstructures in PBS containing 12.5 μg/mL trypsin–EDTA. The inner core was fabricated at a laser power of 60 mW and exhibited red fluorescence, while the outer shells were printed at 45 mW and 30 mW, respectively. Bright-field (Figure 2C) and fluorescence (Figure 2D) microscopy images recorded at different time intervals clearly reveal the gradual degradation of the outer shell, which serves as a sacrificial barrier protecting the encapsulated drugs in the inner core from premature release. The outer shell printed at 30 mW (Figure 2C(i)) degraded first within 60

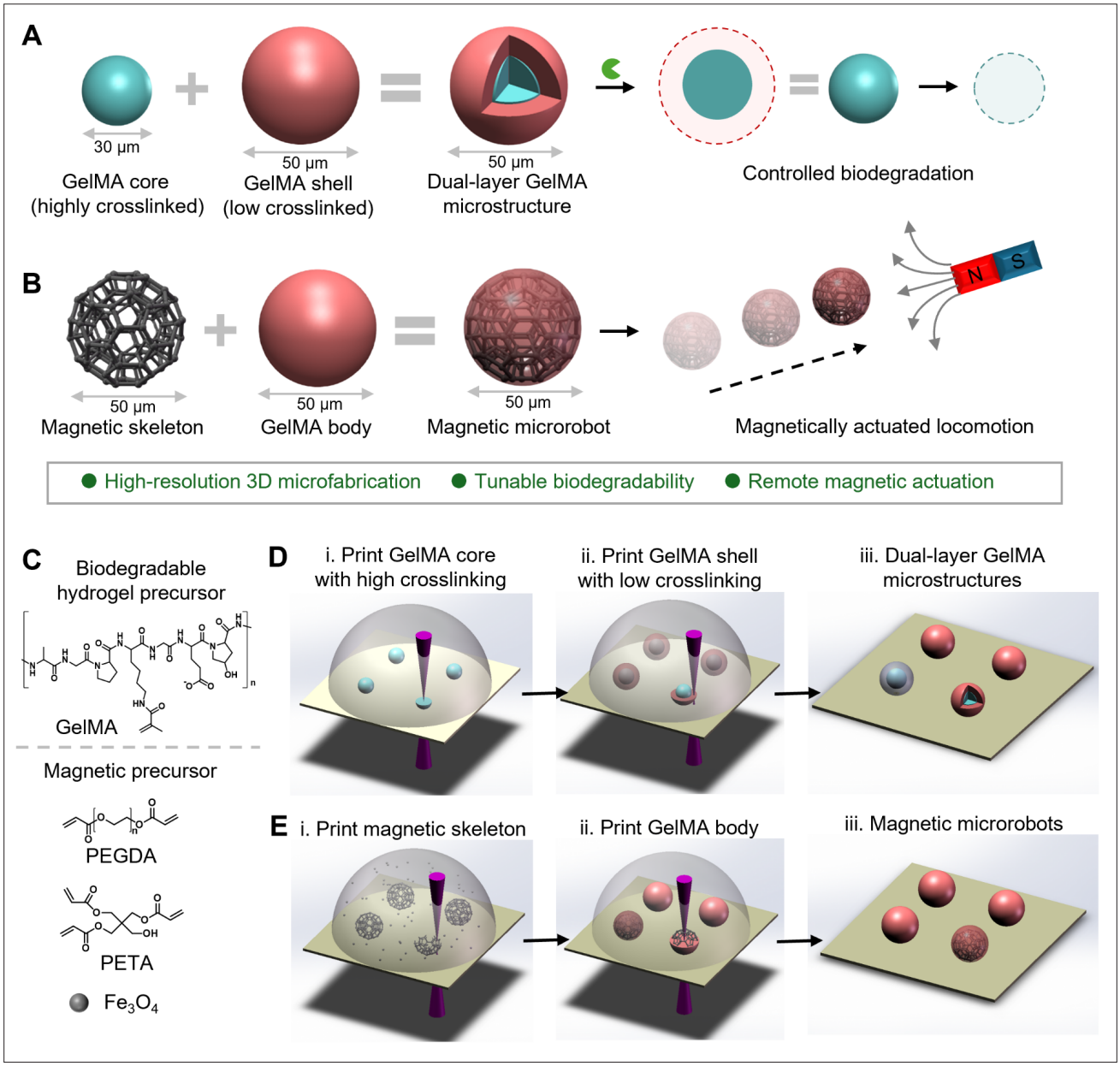

Figure 1. Schematic illustration of the design and fabrication of the biodegradable hydrogel microrobots. (A) Structural design of the dual-layer GelMA microstructures with tunable crosslinking degrees for controlled biodegradation. (B) Structural design of the magnetic microrobots composed of a magnetic skeleton and a GelMA body. (C) Chemical composition of the developed precursors used for 3D printing of dual-layer GelMA microstructures and magnetic microrobots. (D) Schematic representation of the sequential 3D printing process for fabricating dual-layer GelMA microstructures. (E) Schematic representation of the 3D printing process for fabricating magnetically actuated microrobots. Abbreviations: GelMA: Gelatin methacryloyl; PEGDA: Poly(ethylene glycol) diacrylate; PETA: Pentaerythritol tetraacrylate.

minutes (Figure 2C(ii)), delaying the release of fluorescent nanoparticles from the inner core printed at 60 mW until approximately 120 minutes (Figure 2C(iii) and 2D(iii)). In contrast, GelMA microstructures without an outer shell, printed solely at 60 mW, underwent complete degradation and released their fluorescent nanoparticles within the same period (Figure 2C(iii) and 2D(iii)). Notably, GelMA microstructures with an outer shell printed at 45 mW maintained their integrity for a longer duration (Figure 2C(iv)), postponing the onset of release to over 150 minutes (Figure 2D(iv)). As shown in the degradation profiles generated by calculating the average fluorescence intensity per cross-sectional area of the rhodamine-loaded GelMA microstructures (Figure 2E), dual-layer GelMA

microstructures with an outer shell exhibited significantly prolonged degradation compared to those without, confirming the effectiveness of the outer protective layer in delaying degradation and achieving controlled drug release. In addition to laser power, scanning speed can also be used to modulate the crosslinking density. In this study, we maintained a constant scanning speed of 5 mm/s and focused on varying the laser power to achieve different crosslinking levels. Nonetheless, scanning speed represents another viable parameter for adjusting crosslinking density,[61–63] further highlighting the design flexibility of our fabrication process. Compared with previously reported GelMA-based magnetic microrobots,[45–47] our printed dual-layer GelMA microstructures not only exhibit comparable biodegradability and achieve drug release within hours, but also provide an additional advantage: degradability can be further regulated by introducing an outer sacrificial barrier. This design minimizes the risk of early or uncontrolled cargo leakage before the microrobots reach the target site, which would otherwise severely compromise therapeutic efficacy.

3.3. Drug-loading capability and biodegradation of GelMA microstructures

After investigating the controlled degradability of the printed GelMA microstructures, we next evaluated their drug-loading capability and degradation behavior in cellular environments. *In vitro* experiments were conducted to assess the drug-loading capability (using DNA as a model molecule) and biodegradability of the fabricated GelMA microstructures under cell culture conditions. The GelMA microstructures were first dehydrated by freeze drying and subsequently incubated in PBS containing 2 μg of DNA lipoplex overnight. After incubation, the microstructures were rinsed three times with PBS to remove unbound DNA and subsequently co-cultured with cells. After 48 hours, enhanced green fluorescent protein (EGFP) expressing cells were observed under fluorescence microscopy, showing merged images of the GelMA microstructures and EGFP cells (Figure 3A). Figure S3 presents the control group without GelMA microstructures, confirming that green fluorescence signals originated from the DNA-loaded GelMA microstructures shown in Figure 3A. To quantify the DNA loading capacity, 10 μL of trypsin-EDTA was added to samples containing 50 GelMA microstructures (50 μm in diameter) or 100 GelMA microstructures (20 μm in diameter) to induce rapid degradation. The DNA concentration in the degraded solution was then measured using a NanoDrop spectrophotometer (Figure 3B). As expected, the larger 50 μm GelMA microstructures exhibited higher DNA loading than the smaller 20 μm ones due to their greater internal volume and surface area available for adsorption.

The cytocompatibility of the GelMA microstructures was further evaluated by co-culturing them with MC3T3 E1 fibroblasts. The dual-layer microstructures consisted of two GelMA layers fabricated at different laser powers: an inner rhodamine-containing core (30 μm, 45 mW) and an outer shell (50 μm, 30 mW) without rhodamine. The MC3T3 cells were cultured with the GelMA microstructures for one week, and time-lapse microscopy images were recorded to monitor cellular growth and interaction with the GelMA microstructures (Figure 3C). As shown in the figure, MC3T3 cells proliferate rapidly and typically begin adhering and spreading within approximately 3 hours. At 18 hours, most MC3T3 cells exhibit the expected spreading morphology, and only a few early apoptotic events are observed, clearly demonstrating that the rounded morphology at later stages is primarily due to overconfluence rather than poor adhesion or cytotoxic effects. By 42 hours, the cell density in the imaged region had become sufficiently high that individual cells could no longer maintain distinct spreading morphologies. The results indicate that cells adhered to the surface of the GelMA microstructures and continued to proliferate across the culture substrate, demonstrating good cytocompatibility and cell affinity. During culture, partial deformation and degradation of the outer shell were observed in some GelMA microstructures, suggesting gradual enzymatic degradation of GelMA by cell-secreted proteases. Figure 3D compares the shape changes of GelMA microstructures incubated in PBS and cell culture medium. In PBS at 37°C, the GelMA microstructure exhibited minor and uniform expansion, whereas those cultured with cells displayed irregular deformation, likely caused by localized enzymatic activity. Figure 3E further shows the degradation behavior of GelMA microstructures exposed to trypsin–EDTA (125 μg/mL) enzymatic medium. GelMA microstructures without the outer protective layer degraded rapidly and disappeared from their initial positions within 10 minutes, while those with an outer layer, which had already undergone partial degradation during cell culture, were completely degraded at a later stage. These findings confirm that the dual-layer GelMA microstructures possess tunable biodegradation and excellent biocompatibility. Their ability to gradually degrade under enzymatic or cellular conditions, while maintaining structural integrity for controlled cargo release, highlights their strong potential for use in biologically relevant environments for targeted and sustained therapeutic delivery.

3.4. Fabrication and magnetic actuation of GelMA-based microrobots

To fabricate the magnetic microrobots, we designed a magnetic skeleton that could be effectively embedded within the GelMA matrix to enable remote magnetic

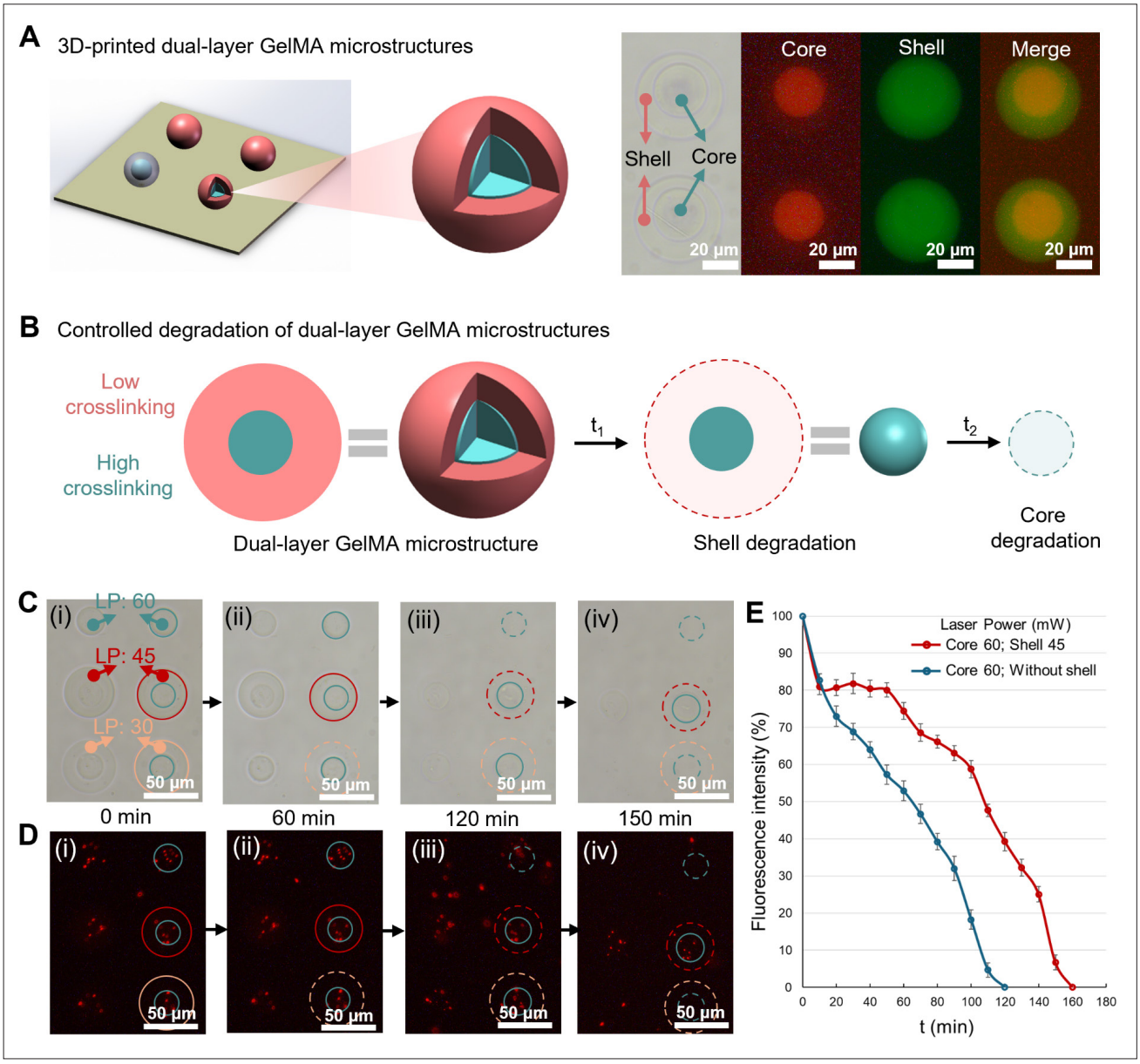

Figure 2. Tunable degradability of printed dual-layer GelMA microstructures. (A) Schematic illustration and microscopy images of the 3D-printed dual-layer GelMA microstructures. (B) Schematic representation of the controlled degradation of GelMA microstructures. (C) Bright-field microscopy images showing the degradation of GelMA microstructures in trypsin–EDTA enzymatic solution. (D) Fluorescence microscopy images showing the controlled release of rhodamine from the GelMA microstructures. (E) Degradation profiles of the 3D-printed GelMA microstructures with and without an outer shell. Data are presented as mean ± standard deviation (SD). Abbreviation: GelMA: Gelatin methacryloyl.

actuation. Figure 4A schematically illustrates the structural design of the magnetic microrobots, together with bright-field and fluorescence microscopy images confirming their successful fabrication. The microrobots consist of an internal magnetic skeleton and a GelMA body, both with a diameter of 50 μm. The magnetic skeleton, composed of PEGDA and PETA integrated with Fe_3O_4 MNPs, exhibits distinct red and blue fluorescence, verifying its successful incorporation within the GelMA body. Figure 4B shows the detachment process of the magnetic microrobots from the glass substrate, as demonstrated in Video S1. The microrobots containing the magnetic skeleton could be easily detached, indicating that the embedded magnetic framework effectively enhances their mechanical stability. In contrast, microstructures fabricated solely from GelMA without the magnetic skeleton appeared soft and adhesive, making them difficult to detach from the glass substrate (Video S2). This comparison clearly demonstrates that

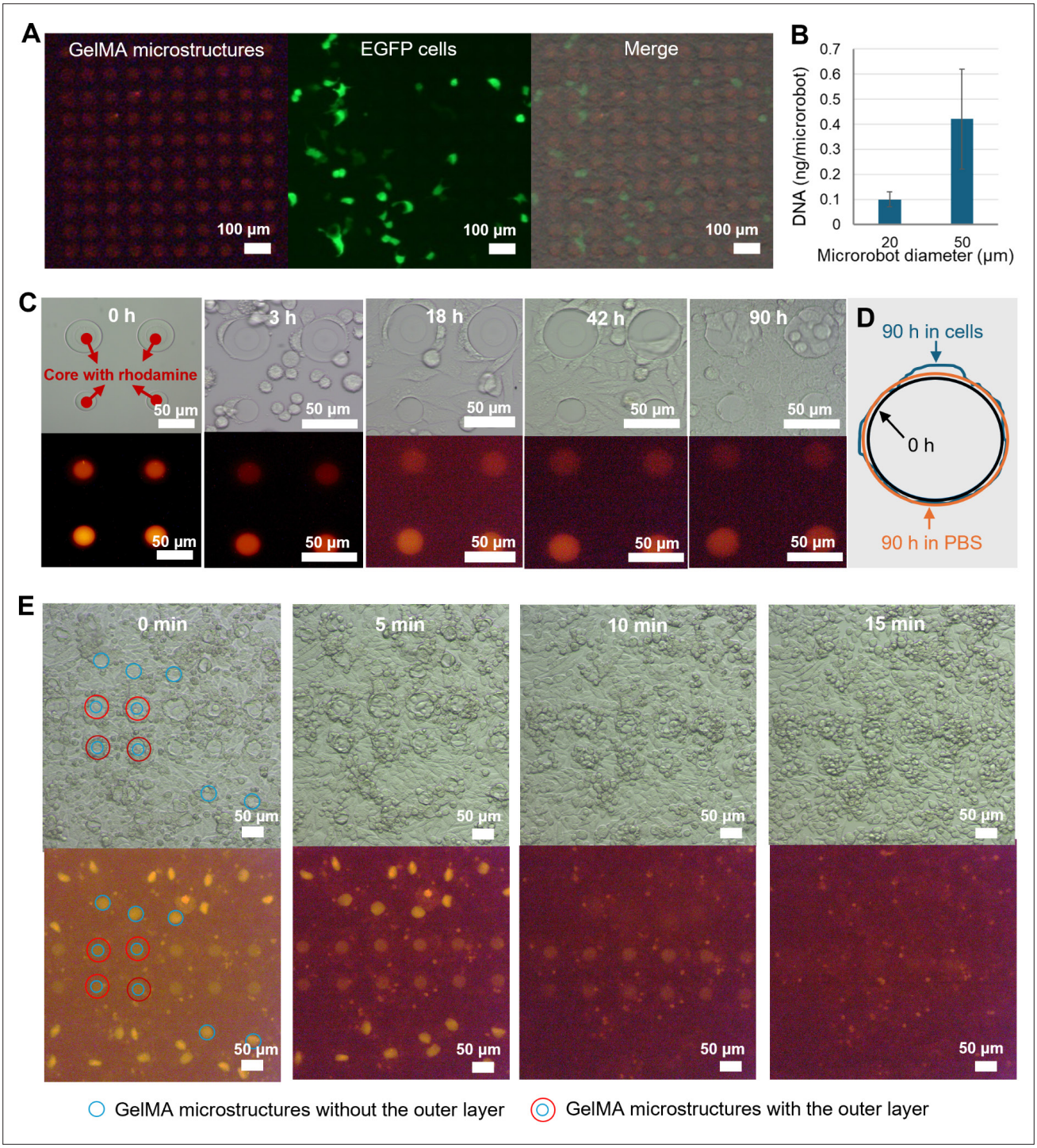

Figure 3. Drug-loading capability and biodegradation of GelMA microstructures. (A) Fluorescence microscopy images showing GelMA microstructures containing rhodamine, EGFP-expressing cells after 48 h co-culture, and merged images of microstructures and EGFP cells. (B) Quantitative analysis of DNA loading capacity on GelMA microstructures of different sizes. Data are presented as mean ± standard deviation (SD). (C) Time lapse images showing microstructures' behavior and cell proliferation during MC3T3 culture. (D) Comparison of GelMA microstructure outlines in PBS and cell culture after 90 h. The black line represents the original outline, while orange and blue lines indicate deformation in PBS and cell culture, respectively. (E) Degradation process of the GelMA microstructures in trypsin–EDTA enzymatic solution. Abbreviations: EGFP: Enhanced green fluorescent protein; GelMA: Gelatin methacryloyl; PBS: Phosphate-buffered saline.

the incorporation of the magnetic skeleton improves the microrobots' structural robustness and handling reliability.

The embedded Fe_3O_4 MNPs within the magnetic skeleton impart strong magnetic responsiveness, as demonstrated in our previous studies,[5,24] enabling precise and remote control of microrobot motion under an external magnetic field (Figure 4C). The locomotion behavior of the microrobots was evaluated under a permanent magnetic field to assess their controllability. As shown in Figure 4D and Video S3, the microrobot exhibited directional locomotion toward the target position in response to the applied magnetic field, demonstrating stable and controlled actuation. Although only linear motion driven by a permanent magnet was demonstrated in this study, more complex trajectories could be achieved under rotating magnetic fields generated by previously reported electromagnetic systems.[24,26,35,64] Such magnetic control strategies could further enable precise navigation of the microrobots through biological fluids and intricate physiological environments.[29,34,64–66] Overall, these results indicate that the developed GelMA-based magnetic microrobots possess excellent controllability, mechanical robustness, and biocompatibility, providing a promising foundation for future *in vivo* applications, including targeted drug delivery, minimally invasive surgery, and localized diagnostic interventions.

4. Conclusion

In summary, we developed 3D-printed biodegradable GelMA-based hydrogel microrobots capable of controlled therapeutic delivery. Using high-resolution direct laser writing, dual-layer GelMA architectures with distinct

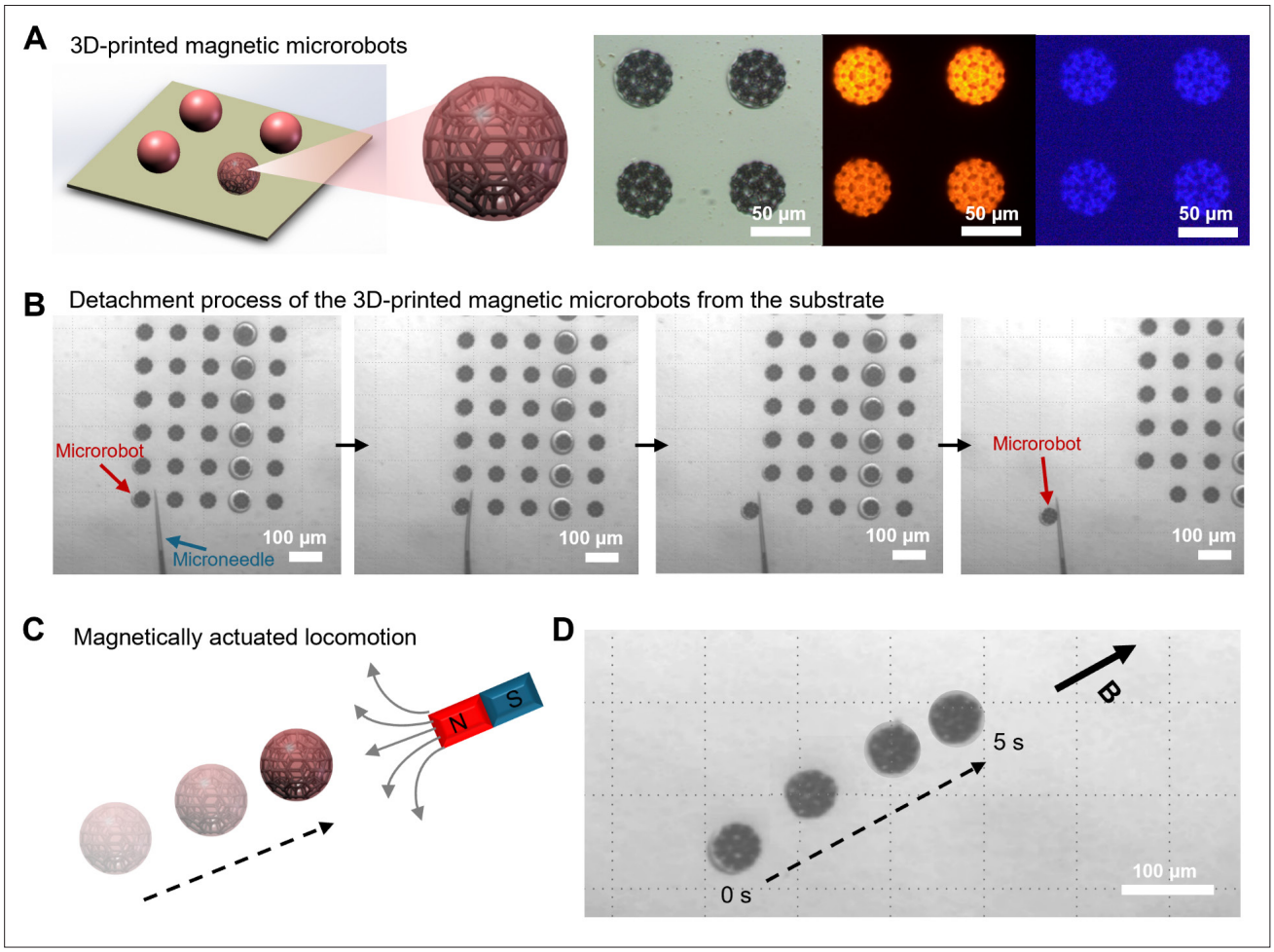

Figure 4. Magnetic actuation of printed GelMA-based microrobots. (A) Schematic illustration along with bright-field, and fluorescence microscopy images of the 3D-printed magnetic microrobots. (B) Microscopy images showing the detachment process of the 3D-printed microrobots from the substrate. (C) Schematic illustration of the magnetic actuation of the 3D-printed microrobots under an external magnetic field. (D) Time-lapse microscopy images showing the magnetically actuated locomotion of the microrobot. Abbreviation: GelMA: Gelatin methacryloyl.

crosslinking degrees were fabricated, enabling tunable degradation and programmable release of encapsulated drugs. The low-crosslinked outer shell serves as a protective barrier, preventing premature release of encapsulated drugs, while the highly crosslinked inner core allows sustained and controllable release upon degradation. The integration of a biocompatible magnetic skeleton composed of PEGDA, PETA, and Fe_3O_4 MNPs provides the microrobots with enhanced mechanical strength and precise magnetic responsiveness, facilitating controlled locomotion under an external magnetic field. These microrobots exhibit excellent biocompatibility and gradual enzymatic degradability, demonstrating their potential as safe and efficient platforms for therapeutic delivery. Overall, this work establishes a versatile strategy for fabricating biodegradable magnetically actuated microrobots, offering new opportunities for targeted drug delivery, tissue engineering, and minimally invasive biomedical interventions.

Although the current system is promising, it still has several limitations. Achieving real-time tracking of microrobot motion and *in situ* monitoring of drug release within deep or dynamic physiological environments remains challenging, yet is crucial for clinical translation. Furthermore, the present study focuses on a single model drug and the delivery of multiple drugs with programmable release profiles at specific times and locations has yet to be realized. Therefore, future research should focus on integrating real-time imaging or sensing modalities to monitor microrobot trajectories and drug release dynamics *in vivo*. The platform should also be expanded to enable the spatiotemporal release of multiple therapeutic agents. Such advancements would further expand the range of applications of biodegradable, magnetically actuated microrobots in targeted drug delivery, tissue engineering, and minimally invasive biomedical interventions.

Acknowledgments

None.

Funding

This work was supported by the Shandong Provincial Natural Science Foundation (Grant No. ZR2025QC1530) and the Taishan Scholars Program.

Conflict of interest

The authors declare they have no competing interests.

Author contributions

Conceptualization: Pan Liao
Formal analysis: Pan Liao, Junyang Li, Shuxun Chen, Yi Hou, Guangda Zhu
Investigation: Pan Liao
Methodology: Pan Liao, Junyang Li, Shuxun Chen
Writing–original draft: Pan Liao, Yi Hou, Guangda Zhu
Writing–review & editing: Pan Liao, Yi Hou, Guangda Zhu, Dong Sun

Ethics approval and consent to participate

Not applicable

Consent for publication

Not applicable

Availability of data

All data are available in the main text or the supplementary materials. Additional data are available from the corresponding author upon request.

References

1. Manzari MT, Shamay Y, Kiguchi H, *et al*. Targeted drug delivery strategies for precision medicines. *Nat Rev Mater.* 2021;6(4):351-370.
doi: 10.1038/s41578-020-00269-6.

2. Huang S, Zhu Y, Zhang L, *et al*. Recent advances in delivery systems for genetic and other novel vaccines. *Adv Mater.* 2022;34(46):2107946.
doi: 10.1002/adma.202107946.

3. Bian X, Zhou L, Luo Z, *et al*. Emerging delivery systems for enabling precision nucleic acid therapeutics. *ACS Nano.* 2025;19(4):4039-4083.
doi: 10.1021/acsnano.4c11858.

4. Yang Z, Xu C, Lee JX, *et al*. Magnetic miniature soft robot with reprogrammable drug-dispensing functionalities: toward advanced targeted combination therapy. *Adv Mater.* 2024;36(48):2408750.
doi: 10.1002/adma.202408750.

5. Wei T, Liu J, Li D, *et al*. Development of magnet-driven and image-guided degradable microrobots for the precise delivery of engineered stem cells for cancer therapy. *Small.* 2020;16(41):1906908.
doi: 10.1002/smll.201906908.

6. Gao J, Xia Z, Gunasekar S, *et al*. Precision drug delivery to the central nervous system using engineered nanoparticles. *Nat Rev Mater.* 2024;9(8):567-588.
doi: 10.1038/s41578-024-00695-w.

7. Tambuyzer E, Vandendriessche B, Austin CP, *et al*. Therapies for rare diseases: therapeutic modalities, progress and challenges ahead. *Nat Rev Drug Discov.* 2020;19(2):93-111.
doi: 10.1038/s41573-019-0049-9.

8. Akhtar A, Andleeb A, Waris TS, *et al*. Neurodegenerative diseases and effective drug delivery: A review of challenges and novel therapeutics. *J Controlled Release.* 2021;330:1152-1167. doi: 10.1016/j.jconrel.2020.11.021.

9. Chen Z, Sánchez MM. Microrobots in gynaecological care and reproductive medicine. *Nat Rev Electr Eng.* 2024;1(12):759-761. doi: 10.1038/s44287-024-00102-0.

10. Nelson BJ, Pané S. Delivering drugs with microrobots. *Science*. 2023;382(6675):1120-1122. doi: 10.1126/science.adh3073.

11. Magdanz V, Khalil ISM, Simmchen J, *et al*. IRONSperm: Sperm-templated soft magnetic microrobots. *Sci Adv.* 2020;6(28):eaba5855. doi: 10.1126/sciadv.aba5855.

12. Wang X, Chen X, Alcântara CCJ, *et al*. MOFBOTS: metal-organic-framework-based biomedical microrobots. *Adv Mater.* 2019;31(27):1901592. doi: 10.1002/adma.201901592.

13. Ju X, Chen C, Oral CM, *et al*. Technology roadmap of micro/nanorobots. *ACS Nano.* 2025;19(27):24174-24334. doi: 10.1021/acsnano.5c03911.

14. Liu D, Wang T, Lu Y. Untethered microrobots for active drug delivery: from rational design to clinical settings. *Adv Healthc Mater.* 2022;11(3):2102253. doi: 10.1002/adhm.202102253.

15. Wang B, Kostarelos K, Nelson BJ, *et al*. Trends in micro-/nanorobotics: materials development, actuation, localization, and system integration for biomedical applications. *Adv Mater.* 2021;33(4):2002047. doi: 10.1002/adma.202002047.

16. Sun M, Wu Y, Zhang J, *et al*. Versatile, modular, and customizable magnetic solid-droplet systems. *Proc Natl Acad Sci.* 2024;121(32):e2405095121. doi: 10.1073/pnas.2405095121.

17. Sun M, Sun B, Park M, *et al*. Individual and collective manipulation of multifunctional bimodal droplets in three dimensions. *Sci Adv.* 2024; 10(29): eadp1439. doi: 10.1126/sciadv.adp1439.

18. Sun M, Yang S, Jiang J, *et al*. Bioinspired self-assembled colloidal collectives drifting in three dimensions underwater. *Sci Adv.* 2023;9(45):eadj4201. doi: 10.1126/sciadv.adj4201.

19. Sun M, Hao B, Yang S, *et al*. Exploiting ferrofluidic wetting for miniature soft machines. *Nat Commun.* 2022;13(1):7919. doi: 10.1038/s41467-022-35646-y.

20. Xia N, Jin D, Yang Z, *et al*. Inverse programming of ferromagnetic domains for 3D curved surfaces of soft materials. *Nat Synth.* 2025;4(5):642-654. doi: 10.1038/s44160-025-00746-2.

21. Yang C, Liu X, Song X, *et al*. Design and batch fabrication of anisotropic microparticles toward small-scale robots using microfluidics: recent advances. *Lab Chip.* 2024;24(19):4514-4535. doi: 10.1039/D4LC00566J.

22. Dong Y, Wang L, Iacovacci V, *et al*. Magnetic helical micro-/nanomachines: Recent progress and perspective. *Matter.* 2022;5(1):77-109. doi: 10.1016/j.matt.2021.10.010.

23. Zhang L, Wang S, Hou Y. Magnetic micro/nanorobots in cancer theranostics: from designed fabrication to diverse applications. *ACS Nano.* 2025;19(8):7444-7481. doi: 10.1021/acsnano.4c10382.

24. Li J, Li X, Luo T, *et al*. Development of a magnetic microrobot for carrying and delivering targeted cells. *Sci Robot.* 2018;3(19):eaat8829. doi: 10.1126/scirobotics.aat8829.

25. Wang Q, Du X, Jin D, *et al*. Real-time ultrasound doppler tracking and autonomous navigation of a miniature helical robot for accelerating thrombolysis in dynamic blood flow. *ACS Nano.* 2022;16(1):604-616. doi: 10.1021/acsnano.1c07830.

26. Dong Y, Wang L, Zhang Z, *et al*. Endoscope-assisted magnetic helical micromachine delivery for biofilm eradication in tympanostomy tube. *Sci Adv.* 2022;8(40):eabq8573. doi: 10.1126/sciadv.abq8573.

27. Sun M, Chan KF, Zhang Z, *et al*. Magnetic microswarm and fluoroscopy-guided platform for biofilm eradication in biliary stents. *Adv Mater.* 2022;34(34):2201888. doi: 10.1002/adma.202201888.

28. Choi J, Hwang J, Kim J, *et al*. Recent progress in magnetically actuated microrobots for targeted delivery of therapeutic agents. *Adv Healthc Mater.* 2021;10(6):2001596. doi: 10.1002/adhm.202001596.

29. Jin D, Yuan K, Du X, *et al*. Domino reaction encoded heterogeneous colloidal microswarm with on-demand morphological adaptability. *Adv Mater.* 2021;33(37): 2100070. doi: 10.1002/adma.202100070.

30. Dong M, Wang X, Chen X, *et al*. 3D-printed soft magnetoelectric microswimmers for delivery and differentiation of neuron-like cells. *Adv Funct Mater.* 2020;30(17):1910323. doi: 10.1002/adfm.201910323.

31. Sun B, Sun M, Zhang Z, *et al*. Magnetic hydrogel micromachines with active release of antibacterial agent for biofilm eradication. *Adv Intell Syst.* 2024;6(2):2300092. doi: 10.1002/aisy.202300092.

32. Terzopoulou A, Wang X, Chen X, *et al*. Biodegradable metal-organic framework-based microrobots (MOFBOTs). *Adv Healthc Mater.* 2020;9(20):2001031. doi: 10.1002/adhm.202001031.

33. Wang B, Chan KF, Yuan K, *et al*. Endoscopy-assisted magnetic navigation of biohybrid soft microrobots with rapid endoluminal delivery and imaging. *Sci Robot.* 2021;6(52):eabd2813. doi: 10.1126/scirobotics.abd2813.

34. Rajabasadi F, Moreno S, Fichna K, *et al*. Multifunctional 4D-printed sperm-hybrid microcarriers for assisted reproduction. *Adv Mater.* 2022;34(50):2204257. doi: 10.1002/adma.202204257.

35. Alapan Y, Bozuyuk U, Erkoc P, *et al*. Multifunctional surface microrollers for targeted cargo delivery in physiological blood flow. *Sci Robot.* 2020;5(42): eaba5726. doi: 10.1126/scirobotics.aba5726.

36. Su L, Jin D, Wang Y, *et al*. Modularized microrobot with lock-and-detachable modules for targeted cell delivery in bile duct. *Sci Adv.* 2023;9(50):eadj0883. doi: 10.1126/sciadv.adj0883.

37. Xin C, Jin D, Hu Y, *et al*. Environmentally adaptive shape-morphing microrobots for localized cancer cell treatment. *ACS Nano.* 2021;15(11):18048-18059. doi: 10.1021/acsnano.1c06651.

38. Chen S, Tan Z, Liao P, *et al*. Biodegradable microrobots for DNA vaccine delivery. *Adv Healthc Mater*. 2023;12(21):2202921. doi: 10.1002/adhm.202202921.

39. Zhang F, Guo Z, Li Z, *et al*. Biohybrid microrobots locally and actively deliver drug-loaded nanoparticles to inhibit the progression of lung metastasis. *Sci Adv.* 2024;10(24):eadn6157. doi: 10.1126/sciadv.adn6157.

40. Llacer-Wintle J, Rivas-Dapena A, Chen X-Z, *et al*. Biodegradable small-scale swimmers for biomedical applications. *Adv Mater.* 2021;22:2102049. doi: 10.1002/adma.202102049.

41. Li J, Yu J. Biodegradable microrobots and their biomedical applications: a review. *Nanomaterials*. 2023;13(10): 1590. doi: 10.3390/nano13101590.

42. He J, Sun Y, Gao Q, *et al*. Gelatin methacryloyl hydrogel, from standardization, performance, to biomedical application. *Adv Healthc Mater.* 2023;12(23):2300395. doi: 10.1002/adhm.202300395.

43. Das S, Jegadeesan JT, Basu B. Gelatin methacryloyl (GelMA)-based biomaterial inks: process science for 3D/4D printing and current status. *Biomacromolecules*. 2024;25(4):2156-2221. doi: 10.1021/acs.biomac.3c01271.

44. Xia B, Liu Y, Xing Y, *et al*. Biodegradable medical implants: reshaping future medical practice. *Adv Sci*. 2025;12(35):e08014. doi: 10.1002/advs.202508014.

45. Wang X, Qin X-H, Hu C, *et al*. 3D printed enzymatically biodegradable soft helical microswimmers. *Adv Funct Mater.* 2018;28(45):1804107. doi: 10.1002/adfm.201804107.

46. Ceylan H, Yasa IC, Yasa O, *et al*. 3D-printed biodegradable microswimmer for theranostic cargo delivery and release. *ACS Nano.* 2019;13(3):3353-3362. doi: 10.1021/acsnano.8b09233.

47. Noh S, Jeon S, Kim E, *et al*. A biodegradable magnetic microrobot based on gelatin methacrylate for precise delivery of stem cells with mass production capability. *Small.* 2022;18(25):2107888. doi: 10.1002/smll.202107888.

48. Landers FC, Hertle L, Pustovalov V, *et al*. Clinically ready magnetic microrobots for targeted therapies. *Science.* 2025;390:6774. doi: 10.1126/science.adx1708.

49. Wong PT, Choi SK. Mechanisms of drug release in nanotherapeutic delivery systems. *Chem Rev.* 2015;115(9):3388-3432. doi: 10.1021/cr5004634.

50. Mitchell MJ, Billingsley MM, Haley RM, *et al*. Engineering precision nanoparticles for drug delivery. *Nat Rev Drug Discov.* 2021;20(2):101-124. doi: 10.1038/s41573-020-0090-8.

51. Paarakh MP, Jose PA, Setty C, *et al*. Release kinetics-concepts and applications. *Int J Pharm Res Technol.* 2023;8(1):12-20. doi: 10.31838/ijprt/08.01.02.

52. Tibbitt MW, Dahlman JE, Langer R. Emerging frontiers in drug delivery. *J Am Chem Soc.* 2016;138(3):704-717. doi: 10.1021/jacs.5b09974.

53. Pinheiro T, Morais M, Silvestre S, *et al*. Direct laser writing: from materials synthesis and conversion to electronic device processing. *Adv Mater.* 2024;36(26):2402014. doi: 10.1002/adma.202402014.

54. Balena A, Bianco M, Pisanello F, *et al*. Recent advances on high-speed and holographic two-photon direct laser writing. *Adv Funct Mater.* 2023;33(39):2211773. doi: 10.1002/adfm.202211773.

55. Jaiswal A, Rastogi CK, Rani S, *et al*. Two decades of two-photon lithography: Materials science perspective for additive manufacturing of 2D/3D nano-microstructures. *iScience*. 2023;26(4):106374. doi: 10.1016/j.isci.2023.106374.

56. O'Halloran S, Pandit A, Heise A, *et al*. Two-photon polymerization: fundamentals, materials, and chemical modification strategies. *Adv Sci.* 2023;10(7):2204072. doi: 10.1002/advs.202204072.

57. Wang H, Zhang W, Ladika D, *et al*. Two-photon polymerization lithography for optics and photonics: fundamentals, materials, technologies, and applications. *Adv Funct Mater.* 2023;2214211.

doi: 10.1002/adfm.202214211.

58. Jia X, Fan X, Chen C, *et al*. Chemical and structural engineering of gelatin-based delivery systems for therapeutic applications: a review. *Biomacromolecules*. 2024;25(2):564-589. doi: 10.1021/acs.biomac.3c01021.

59. Mamidi N, Ijadi F, Norahan MH. Leveraging the recent advancements in GelMA scaffolds for bone tissue engineering: an assessment of challenges and opportunities. *Biomacromolecules*. 2024;25(4):2075-2113. doi: 10.1021/acs.biomac.3c00279.

60. Jiao W, Shan J, Gong X, *et al*. GelMA hydrogel: A game-changer in 3D tumor modeling. *Mater Today Chem*. 2024;38:102111. doi: 10.1016/j.mtchem.2024.102111.

61. Drobecq I, Bigot C, Soppera O, *et al*. Optimizing dimensional accuracy in two-photon polymerization: Influence of energy dose and proximity effects on sub-micrometric fiber structures. *Addit Manuf.* 2025;103:104735. doi: 10.1016/j.addma.2025.104735.

62. Bornillo K, Sorgato M, Lucchetta G. Optimizing two-photon polymerization for rapid and high-resolution prototyping of low-friction microtextured surfaces. *Prog Addit Manuf.* 2025;10(9):5977-5992. doi: 10.1007/s40964-025-00947-3.

63. Fu H, Yu B. 3D micro/nano hydrogel structures fabricated by two-photon polymerization for biomedical applications. *Front Bioeng Biotechnol.* 2024;12:1339450. doi: 10.3389/fbioe.2024.1339450.

64. Dong Y, Wang L, Yuan K, *et al*. Magnetic microswarm composed of porous nanocatalysts for targeted elimination of biofilm occlusion. *ACS Nano.* 2021;15(3):5056-5067. doi: 10.1021/acsnano.0c10010.

65. Xu H, Medina-Sánchez M, Schmidt OG. Magnetic micromotors for multiple motile sperm cells capture, transport, and enzymatic release. *Angew Chem Int Ed.* 2020;59(35):15029-15037. doi: 10.1002/anie.202005657.

66. Liu D, Guo R, Wang B, *et al*. Magnetic micro/nanorobots: a new age in biomedicines. *Adv Intell Syst*. 2022;4(12):2200208. doi: 10.1002/aisy.202200208.